HHS Public Access

Author manuscript

Methods Mol Biol. Author manuscript; available in PMC 2021 February 23.

Published in final edited form as:

Methods Mol Biol. 2017 ; 1529: 323–352. doi:10.1007/978-1-4939-6637-0_17.

A Protocol for the Design of Protein and Peptide Nanostructure Self-Assemblies Exploiting Synthetic Amino Acids

Nurit Haspel[1], **Jie Zheng**[2], **Carlos Aleman**[3,4], **David Zanuy**[3], **Ruth Nussinov**[5,6,7]

[1]Department of Computer Science, The University of Massachusetts Boston, 100 Morrissey Blvd., Boston, MA, 02125, USA.

[2]Department of Chemical and Biomolecular Engineering, The University of Akron, Akron, OH, 44325, USA.

[3]Departament d'Enginyeria Química, E. T. S. d'Enginyeria Industrial de Barcelona, Universitat Politècnica de Catalunya, Diagonal 647, 08028, Barcelona, Spain.

[4]Center for Research in Nano-Engineering, Universitat Politècnica de Catalunya, Campus Sud, Edifici C', C/Pasqual i Vila s/n, E-08028, Barcelona, Spain.

[5]Department of Human Genetics and Molecular Medicine, Sackler School of Medicine, Sackler Inst. of Molecular Medicine, Tel Aviv University, Tel Aviv, 69978, Israel.

[6]Basic Science Program, Leidos Biomedical Research, Inc., Frederick, MD, 21702, USA.

[7]Cancer and Inflammation Program, National Cancer Institute, Frederick, MD, 21702, USA.

Abstract

In recent years there has been increasing interest in nanostructure design based on the self-assembly properties of proteins and polymers. Nanodesign requires the ability to predictably manipulate the properties of the self-assembly of autonomous building blocks, which can fold or aggregate into preferred conformational states. The design includes functional synthetic materials and biological macromolecules. Autonomous biological building blocks with available 3D structures provide an extremely rich and useful resource. Structural databases contain large libraries of protein molecules and their building blocks with a range of sizes, shapes, surfaces, and chemical properties. The introduction of engineered synthetic residues or short peptides into these building blocks can greatly expand the available chemical space and enhance the desired properties. Herein, we summarize a protocol for designing nanostructures consisting of self-assembling building blocks, based on our recent works. We focus on the principles of nanostructure design with naturally occurring proteins and synthetic amino acids, as well as hybrid materials made of amyloids and synthetic polymers.

Keywords

Nanostructures; Self-assembly; Peptide-based nanodesign; Synthetic amino acids; Beta-helical proteins; Computational nanodesign; Amyloid peptides; Hybrid materials

nurit.haspel@umb.edu.

1 Introduction

Nanotechnology aims to design novel materials and molecular devices, often by exploiting the natural ability of molecules to self-assemble into larger, ordered structures at the nanoscale. Nanotechnology applications include targeted drug delivery systems, computational devices, and scaffolding tissues [1–3]. In nature, protein domains often self-assemble, spontaneously organizing in stable higher-order structures through noncovalent interactions. These molecules may create large complexes of well-defined structures and functions. The shapes, sizes, and functions of these structures are determined by the amino acid sequence of these proteins [4, 5]. In recent years there has been much focus on the experimental and computational design of self-assembled nanomaterials based on the self-assembly properties of proteins. Exploiting the natural ability of macromolecules to self-assemble can be a very useful approach in the design and construction of novel molecular structures [5–8]. Much work has been done in recent years in the design and construction of nanostructures using DNA, RNA, and protein segments [9–14]. Advances in peptide synthesis and molecular engineering techniques have made self-assembly of peptide segments a favorable route by which to obtain nanostructures [5, 15–17], particularly those consisting of single or associated tubes, fibers, and vesicles.

Computational methods have become a powerful tool in nanobiology and nanostructure design. The use of advanced simulation methods and efficient modeling algorithms, in addition to the rapidly increasing amount of data in DNA, RNA, and protein databases, can considerably accelerate the design process via fast probing of many possible models in a high-throughput cost-effective way, aiming to experimentally test only feasible models. In this chapter we describe a computational and experimental protocol, based on our previous and current work. We first introduce a protocol for designing self-assembled nanostructures from naturally occurring protein motifs, followed by structural enhancement by synthetic amino acids. Next, we introduce a related method to construct nanostructures based on amyloid peptides. Finally, we introduce a protocol to design hybrid materials based on the conjunction of functional amyloids and synthetic polymers.

2 Computational Nanodesign

Construction of stable nanostructures using natural building blocks is a reasonable and promising strategy toward precisely and quantitatively controlling the supramolecular assemblies. A building block is a well-defined secondary structural unit which, if cut from the protein chain and placed in solution, is still likely to have a conformation similar to the one it has when embedded in the native protein structure. The Protein Data Bank (PDB) is populated by an extensive repertoire of building blocks, with different shapes, sizes, and chemical properties which can be used in rational design of protein-based nanostructures [18]. Some naturally occurring proteins contain a tubular or fibrillar motif in their folds. A good example of tubular proteins is the β-helix protein fold. The fold of β-helical proteins contains a repetitive helical strand-loop motif [19], where each repeat contributes a strand to one or more parallel β-sheet(s). The left-handed β-helical fold is especially suitable: the tubular structure is regular and symmetrical and is often stabilized by a network of interactions between similar residues in consecutive coils [20] (*see* Fig. 1).

The common types of interactions in β-helices include:

1. Asparagine (or glutamine) ladders that stabilize the helical structure through hydrogen bonds between residues in consecutive rungs (Fig. 1a).
2. Stacking of aromatic (Phe, Tyr, His) and aliphatic (Pro) rings (Fig. 1b).
3. Hydrophobic interactions (especially Val, Ile, Leu) (Fig. 1c).

The tubular nature of left-handed β-helical proteins makes them excellent candidates to be used as building blocks to construct fibrillar or tubular nanostructures without the need to perform many structural manipulations. In addition, their helical and symmetric structure makes them good candidates to be excised and tested as modules.

In our work [21] we presented a general approach to the design of nanostructures based on the potential assembly property of protein segments, in which the segments are taken from naturally occurring proteins and have preferred conformational tendencies. We designed nanoconstructs based on left-handed β-helical proteins by selecting short (two turns), repetitive motifs and extracting the corresponding coordinates from the PDB [22]. We assembled copies of the motifs on top of one another so that the assembled nanotube had an almost perfect equilateral triangular shape, with each side being ~18 Å. We simulated the nanostructures using molecular dynamics (MD) to test their structural stability over time. Figure 2 illustrates a schematic flowchart of the process. *Our design principle* is that if the nanostructures can preserve their tube organization and motif association during the simulations, they are promising candidates for experiment. Otherwise, if the nanostructures cannot preserve their original organization in the simulations, they are unlikely to preserve their organization in experiment as well. For those unstable nanostructures, in a subsequent stage (*see* next sections) we reduced the conformational freedom by introducing restricted synthetic residues in strategic positions to improve the structural stability of the designed nanostructures. For a successful design, it is desirable that the substitutions retain both favorable packing interactions and hydrogen bonding with the neighboring residues. Of the 17 systems that we tested, the construct based on the assembly of copies of residues 131–165 of galactoside acetyltransferase from *E. coli* (PDB code: 1krr, chain A) was very stable over the simulation time under all of the tested temperature and ionic strength conditions. Figure 2 shows the sequence and structure of the 1krr system. To assess the structural stability of our tested models, we looked at the retention of the structural organization over time. We largely focused on the organization of the loop regions since these are typically the least stable. We also studied the effect of specific amino acids and chemical interactions on the conformational stability of the structure, focusing again on loop regions. Through mutational study, we found that apart from the characteristic inter-strand interactions of β-helical proteins, the presence of proline residues around the loop areas greatly contributes to the retention of the loop structure and hence to the stability of the overall conformation. In addition, in many cases we found a relatively large number of glycines in loop regions. These glycines were involved in hydrogen bonds with the side chains of other residues in their vicinity and hence contributed to maintaining the conformation of the loops. We next aimed to further enhance the stability of the system by inserting specific point mutations using noncoding amino acids whose structures are available. The choice of such conformationally restricted residues and the positions of insertion were guided by our

mutational observations on the stabilizing effects of naturally occurring residues on the entire system. This work is described in more details below.

We next aimed to modify the 1krr-based nanostructure [23] toward useful biological functions. The original construct is characterized by an internal hydrophobic core, containing mainly valine and isoleucine residues, rendering it inappropriate for the transfer of matter or charge. Since the hollow space inside the structure was narrow and unsuitable for the transport of large molecules, charge transfer seemed to be a feasible application. However, to allow charge transfer we had to modify the chemistry of the internal core of the structure. Charge can be transferred through π-electron stacking or through H1 transfer. Although charge transfer cannot be modeled through classical mechanics, this methodology was appropriate to assess its feasibility. We considered two different scenarios for charge transfer: (1) formation of ladders of π-electron-rich functional groups by substituting some of the original residues in the interior of the construct by other residues capable of π-stacking; and (2) the generation of proton transfer environment through a network of salt bridges, reminiscent of the serine protease catalytic triad. The two necessary conditions to achieve this goal are:

1. The mutated structures must still retain their tubular structuresin the simulation.
2. There must be a side-chain distribution that allows these chemical processes.

To create a ladder of π-stacking residues and to test whether this would affect the structural organization, we inserted a row of histidine residues in each of the three beta-sheets, one sheet at a time (*see* Fig. 2b for an illustration of an example, the histidine mutant) and simulated the mutated structures. Histidine is an aromatic amino acid capable of π-stacking. Its side chain is fairly similar to the size of valine and isoleucine so no drastic steric hindrance or structural changes were expected to occur. The pKa of histidine is six, so in a physiological pH it can assume both a neutral and a charged form with a relatively high probability. Moreover, its neutral form corresponds to equilibrium between two states: one with d hydrogen (ND) protonated and the other with e hydrogen (NE) protonated. This allowed us to test different possible combinations of ionization states. Naturally, we could not sample all possible ionization states due to computational time limitations, but we tried to sample as many as possible as well as different combinations of ionization states. We identified a position where, despite the insertion of histidine, the simulated nanostructures retained their initial organization to a reasonable extent and created a configuration made of networks of neutral histidine, charged histidine, and aspartate, imitating the serine protease catalytic triad. We suggested a structure with a π-stacked row of alternatively neutral and charged histidine residues that interact with a row of aspartate residues through salt bridges, and thus provided the conditions for creating a nanosystem potentially capable of charge transfer.

2.1 Nonstandard Amino Acids

The catalog of amino acids available nowadays for materials sciences applications has rapidly expanded. Only in natural structures, there can be found more than 700 different amino acids [24, 25] (most of them, also L-amino acids) beyond the 20 genetically coded L-amino acids that are contained in proteins. Furthermore, many others have been imagined

and synthesized by organic chemists [24–28]. All those compounds are named under a common designation of nonproteinogenic or noncoded amino acids (nc-aa). Although they are not involved in ribosomal synthesis of native peptides and proteins, several naturally occurring peptides and proteins contain nc-aa [29, 30]. The majority are the results of post-translational modifications that active proteins undergo upon release from the ribosome. Most of these chemical modifications have been found to play crucial roles in both the regulation of metabolic routes and genomic expression. The part played by citrullination (conversion of arginine residue to citrulline) in the relaxation of chromatin and the modulation of the pluripotency of stem cells is especially noteworthy [26].

Currently the use of such molecules stretches over almost all fields of applied natural sciences. They are applied to improve the pharmacological profile of natural peptides endowed with biological activity [31, 32] (to confer resistance against enzymatic degradation, enhance membrane permeability, or increase selectivity and affinity for a particular receptor), and are responsible for the development of nonpeptidic drugs [33]. On the other hand, nc-aa have recently been used in biotechnology for protein reengineering [34, 35]. Thus, proteins containing such residues can acquire new chemical features such as fluorescence [36, 37], redox-activity [38], photosensitivity [37, 39], and specific chemical reactivity [40]. Those new spectroscopic properties [41] can be used as biosensors, spectroscopic or biophysical probes, or even for building new nanosystems for drug delivery and diagnosis through imaging to be used in medicine [34, 40, 42, 43]. Other applications of Nc-aa are their use in nanobiology to promote the self-assembly of nanostructures [44, 45] or for developing bioinspired synthetic organic polymers that emulate the shape and properties of natural peptides and proteins [46, 47].

2.2 Structurally Restricted Amino Acids

Practical use of nc-aa is frequently hampered by the high degree of dispersion that their relevant conformational data present. The most accurate information is extracted from first principle calculations, which are typically reported in physical chemistry journals, whereas their synthetic details are dispersed among specialized journals of organic chemistry. Moreover, spectroscopic and structural studies of small peptide containing nc-aa are generally performed by organic and peptide chemists and their findings are away from biology specialized journals. However, most applications of nc-aa are developed and tried by researcher working on fields related with medicine, protein science, or materials engineering. The lag of systematically correlated information and the great potential applicability of nc-aa led us to integrate these diverse existing contributions into a unified and simple informatics tool that should facilitate the universal use of nc-aa in practical applications. This new database contains the conformational descriptors of any nc-aa ever studied and any relevant bibliographic information about already reported practical uses. The NCAD (Non-Coded Amino acids Database) [48] is a database designed to identify the most suitable nc-aa for any given structural motif, compatibility required for any use in both life and materials sciences. Our tool integrates all structural and energetic descriptors previously reported using quantum mechanics calculations for each nc-aa. A summary of the information integration in the database is presented in Fig. 3. Per each amino acid NCAD contains its complete structural profile, which includes a detailed description of each

minimum energy conformation (dihedral angles, three-dimensional structure, relative energy, etc.) and, if available, all the bibliographic information related to experimental data, included all reported applications (both in bioscience and materials science).

Since simulations can quickly probe many models and provide potentially good candidate nanostructures in terms of structural stability and minimum free energy for experimental test, they could accelerate the design process.

2.2.1 Application to β-Helices Motifs—To enhance the thermodynamic stability of a given β-helical repeat sequence, we engineered chemically constrained residues with backbone conformational tendencies similar to those of natural amino acids in the most mobile (loop) regions. Among the synthetic residues that our group has prepared and studied, here we focused on 1-aminocyclopropanecarboxylic acid (Ac_3c), a simple cyclic *R,R*-dialkylated amino acid with strong stereochemical constraints induced by the highly strained cyclopropane ring. We also tested its double-phenyl derivative, 1-amino-2,2-diphenylcyclopropanecarboxylic acid (c_3Dip), a cyclopropane analogue of phenylalanine bearing two germinal phenyl rings. However, this substitution was unsuccessful, due to the steric effects induced by the residue side chain size.

2.2.2 Survey of Ac_3c Derivatives—Ac_3c is the simplest achiral C-α-tetra-substituted α-amino acid with Cα↔Cα cyclization (Fig. 4). The stereochemical constraints of this amino acid are produced by the unfavorable steric interaction of the two β-methylene groups and by the three-membered ring rigidity. The conformational preferences of Ac_3c were characterized by energy computations of the monopeptide [49–51] and X-ray diffraction analyses [52–55] of a variety of peptides of this residue up to the tetramer level. These studies illustrated that the Ac_3c amino acid prefers the “bridge” region of the Ramachandran map, i.e., $\varphi, \psi \approx \pm 80°, 0°$, which corresponds to position $i + 2$ of type I/I′ and type II/II′ β-turns. Theoretical studies indicated that the tendency of Ac_3c to adopt a small value of ψ is due to the hyper-conjugation between the lone pairs of the carbonyl oxygen of the residue and some adjacent molecular orbitals associated with the C-β-C-β′ bond [56]. This conjugative ability of the Ac_3c cyclopropyl moiety was demonstrated by X-ray crystallography. The N-Cα and Cα-C bond lengths are significantly shortened compared to Cα-tri-substituted and Cα-tetra-substituted α-amino acids [57], and the mean exocyclic N-Cα-C bond angle is significantly larger (116–118°) than the tetrahedral angle (109.5°). Thus, the strong tendency of Ac_3c to adopt β-turn conformations is enhanced by specific intra-residue electronic interactions.

Incorporation of selectively oriented side-chain substituents into conformationally restricted amino acids allows increased control of the backbone fold [58]. Cyclopropane analogues of phenylalaline are particularly attractively because the rigidly oriented phenyl side groups may interact with the backbone sterically and electronically through the aromatic π-orbitals [53, 55, 59]. The side chain orientation of 1-amino-2-phenylcyclopropanecarboxylic acid (c_3Phe) stereoisomers drastically affects the backbone conformational preferences, with a tendency to adopt folded conformations [56, 60, 61]. This tendency was observed in the stereoisomers of 1-amino-2,3-diphenylcyclopropanecarboxylic acid with the phenyl substituents in a *trans* relative disposition (c_3DiPhe) [59, 62] in both solid state and solution.

A cyclopropane analogue of phenylalanine bearing two geminal phenyl side substituents was recently incorporated into Pro-c_3Dip. X-ray diffraction analysis showed that the (*S*)-Pro-(*R*)-c_3Dip stereoisomer adopts two consecutive γ-turns stabilized by intramolecular hydrogen bonds [63]. The ability of c_3Dip to adopt a γ-turn and to induce this structural motif in neighboring amino acids was explained by calculations [64]. The dihedral angle ψ values for all cyclopropane analogues of phenylalanine are close to 0° due to the presence of hyper-conjugative effects [56, 62, 64]. It is worth noting that interesting supramolecular structures have been characterized for peptides rich in c_3Dip [65, 66]. Here we focused on Ac_3c, the simplest Cα-tetra-substituted cyclic *R*-amino acid promoting β-turn-type conformations, and c_3Dip (Fig. 4), in which the Ac_3c conformational preferences are guided toward the γ-turn. Force field parameters for Ac_3c and its derivatives were explicitly developed [50, 51].

To test our design principle, we built two nanotubes using two different motifs of 1krr and 1hv9, both of which adopt similar left-handed β-helical conformation. When submitting the two nanotubes to MD simulations, it can be seen clearly in Fig. 5 that the 1krr nanotube with four repeat β-helical units can well preserve its original tubular structure and display high structural stability (Fig. 5a, b). Moreover, 1krr nanotube bundle—containing three β-helical segments forming a trimeric structure along a threefold screw axis—can retain both the individual tubular structure and the overall trimeric structure. Conversely, the 1HV9 nanotube completely lost the initial, compact nanotubular structure, and all β-helical units started to separate from each other (Fig. 5c). Further structural analysis has determined the most unstable residues at the turn region. Based on our design principle, we replaced two turn residues of Asn5 and Ala27 with the conformationally restricted 1-aminocyclopropanecarboxylic acid (Ac_3c) residue, and the mutated 1hv9 nanotube were able to retain its original tubular structures and displayed very high structural stability (Fig. 5d). Compared to the unstable wild-type 1hv9 nanotube, the enhanced stability originates not only from the increasing number of hydrogen bonds and hydrophobic contacts between each building subunit, but also from the reduced flexibility in the loop regions induced by Ac_3c within each building subunit. Thus, the Ac_3c geometrical confinement effect is sequence-specific and position-specific.

2.2.3 Simulation Protocol—Calculations were performed by using the NAMD package [67]. All of the atoms of the system were considered explicitly, and the energy was calculated by using the CHARMM22 force field [68]. Water molecules were represented explicitly, by using the TIP3 model [69]. The simulations were performed by using the NVT ensemble in an orthorhombic simulation box. We chose constant volume simulations because all of the trajectories were obtained at high temperature. By these means, we could ensure that proper density distribution would not be lost due to thermal effects. Periodic boundary conditions were applied by using the nearest image convention. The box size was adjusted to fit the complex size, so that infinite dilution conditions would be maintained. The box dimensions were adjusted to ($50 \times 50 \times 70$ Å^3) to ensure infinite dilution. Each system contained approximately 15,000–20,000 atoms, including the solvent. The starting molecular structures were built by using the INSIGHTII molecular package (2000, Accelrys, San Diego, CA). For any given arrangement, we fixed the inter-turn distance of adjacent repetitive units to match the inter-strand distance within each unit, which was approximately

4.5 Å. The charge of all potential titratable groups was fixed to those values corresponding to neutral pH, such that all aspartic acid side chains were represented in their anionic form and all lysine side chains in their acidic positively charged form. Both peptide edges were capped to avoid interactions between adjacent termini.

2.2.4 The Simulation Conditions—We performed the simulations under the following conditions:

1. No ions in the solution, 300 K.
2. No ions in the solution, 360 K.
3. Ionic strength of 0.23 % w/w, 300 K (approx. 8 ions).
4. Ionic strength of 0.5 % w/w, 300 K (approx. 16 ions).
5. Ionic strength of 0.8 % w/w, 300 K (approx. 24 ions).

In the case of ionized solution, we kept the overall charge of the system neutral for the use of EWALD particle mesh summation [70] to calculate the electrostatic charges. The ions were chloride and sodium.

Before running each molecular dynamics simulation, the potential energy of each system was minimized by using 5000 conjugate gradient steps. The heating protocol included 15 ps of increasing the temperature of the system from 0 K to the final temperature of 300 K (or 18 ps of increasing the temperature from 0 to 360 K) plus 100 ps of an equilibration period. We perform the simulations at 300 and 360 K in order to enhance the stability differences between the models by means of thermal stress. Furthermore, using high temperature allowed us to infer some kinetic tendencies. Residue-based cutoff was applied at 14 Å, i.e., if any two molecules have any atoms within 14 Å, the interaction between them is evaluated. A numerical integration time step of 1 fs was used for all of the simulations. The nonbonded pair list was updated every 20 steps, and the trajectories were saved every 1000 steps (1 ps) for subsequent analysis. Each simulation was run for a period of 20 ns. Potentially stable systems were run for an additional 20 ns.

We have used this protocol for a few years [21, 23, 71–76] and observed that its results correspond to experimental observations [77–80].

2.2.5 Structural Analysis—We calculated the structural conservation in the following ways:

- Conservation of the size of the structure with respect to the minimized structure: the trajectories were aligned with the initial structure, and the RMSD was calculated with respect to C-α atoms.
- Conservation of the loops was defined as the RMSD of the Cα of each residue of the loop with respect to the initial minimized structure. In addition, the distribution of the backbone dihedral angles was plotted.
- Sequence alignment and analysis were performed with the CLUSTALX software [81].

3 Introduction to Hybrid Materials Based on Amyloid-PLA Conjugates

Hybrid materials are one of the most active areas in biomaterials science. This is because by combining different types of molecules it is possible to merge their properties into new useful chimeric compounds. In the particular case of peptide-polymer conjugates, which result from the covalent integration of a peptide with a synthetic polymer block, they are especially attractive because this kind of hybrid macromolecules combines unique properties that come from the precise chemical structure and functionality of peptides and the stability, functions, and processability of synthetic polymers [82, 83]. The conformational profile of peptide-polymer hybrid compounds has a crucial importance due to its influence on many other parameters such as binding affinity and bioactivity. The conformational landscape of new conjugated macromolecules cannot be understood only in terms of a simple addition of their parts; rather, the dynamic interactions between them should also be considered. Thus, conformational exploration needs to be carried out for the whole system and for its separate components, and the results have to be compared. The huge number of feasible combinations of the conformational states of each of the molecular components dramatically increases the complexity of the problem. Theoretical chemistry tools provide a feasible approach for conformational exploration, since they allow performing the search in a faster, more efficient manner. Diblock copolymers that covalently link proteins and synthetic polymers are among the most promising chimeras, being the subject of intense research using both synthetic and theoretical approaches.

Self-aggregating proteins are found in several pathological processes and are also a target in material science due to their ability to spontaneously form ordered materials with useful physicochemical and mechanical properties [84]. Arginine-Vasopressin (hereafter Vas) and Neuromedin-K (also known as Neurokinin B, and hereafter abbreviated Neuro) are among those peptides that are known to self-aggregate. Vas is a peptidic human hormone involved in the pathogenesis of neurohypophyseal diabetes insipidus (NDI) by aggregating into amyloid-like microfibrils; Neuro is a member of the tachykinins protein family that plays an important role as a neurotransmitter and neuroregulator with the ability to form fibrils resembling amyloids [84]. Neuro has been shown to decrease neuronal damage caused by beta-amyloid protein aggregation by interfering in this molecular process. These two peptides have an intrinsic ability to form self-aggregating self-structured biomaterials both in vivo and in vitro; however, immunological problems may arise due to their proteinogenic nature. On the other hand, poly(*R*-lactic acid) (*R*-PLA, also known as PDLA) is a semi-crystalline biodegradable and biocompatible polyester that has physicochemical properties suitable for making release-controlled systems and tissue engineering scaffolds. These features make *R*-PLA a suitable candidate for introducing biocompatible components by conjugating it to these other molecules. Formation of hybrid conjugates by combining peptides (and proteins) with synthetic polymers result in chimeras (i.e., artificial biomolecules) with a useful set of features, where each component has different sets of properties. The capability of peptides and proteins to self-organize into supra-molecular arrangements complements the inherent tendency of *R*-PLA to similarly self-organize at the supra-molecular level. This polyester has a crystallinity of around 37 %, a glass transition temperature between 60 and 65 °C and a melting temperature between 173 and 178 °C. The

fusion of such properties may lead to novel macromolecules capable of self-aggregation and self-organizing while preserving the key properties of biodegradability and biocompatibility [85].

In a recent work [86] we used computational methods to characterize the conformational preferences of two new hybrid materials derived from the conjugation of Vas and Neuro to a 150 residues-long *R*-PLA chain. Determination of the influence of the polymer component on the conformational preferences of the peptide component is a key question for peptide-mediated self-aggregation, since the conformation of the peptide has a strong impact on such processes. Our study focused on the hypothesis that noncovalent self-aggregation involving tight binding to a hairpin-like backbone conformation enables amyloid formation. Thus, the conformational profiles of the free peptides were first assessed so it can be compared with the conformational profile of the polymer-linked peptide. The comparison between the free peptides and the peptides linked to a model polymer provided an initial benchmark for studying novel potentially self-aggregating materials. Our approach relied on the premise that similar conformational behavior of the free and the polymer-linked peptides, is expected to lead to similar properties. Next we investigated the properties of the polymer when isolated and when conjugated to the peptides to ascertain that it also retains its global properties. Here, we briefly describe the conformational characterization of two amyloidogenic peptides and two new chimeric molecules combining the properties of amyloidgenic peptides and polymers. The study of these specific cases allowed us to model new peptide-polymer chimeras based on general trends observed in studies such as the one presented here. This work set the path for further theoretical and experimental work not only to address the peptide and polymer self-aggregation but also to develop new biomaterials with advanced properties.

Details of the preparation and characterization at the molecular level of the peptide-polymer conjugates resulting from the combination of FF and poly(L-lactide) (PLA), hereafter denoted FF-PLA were described elsewhere [87]. Conjugates based on biodegradable PLA, which is obtained from renewable resources, are expected to present important medical and biotechnological applications. PLAs are produced by ring-opening polymerization (ROP) of lactides and the lactic acid monomers used are obtained from the fermentation of sugar feed stocks. The different stereoisomeric PLA grades, which are produced from L-, D-, and D,L-lactides, can be used in biomedical devices (e.g., scaffolds and drug delivery systems) in which they slowly hydrolyze back to lactic acid and reenter the Krebs cycle. Fan et al. [88] described the synthesis of L-phenylalanine-terminated PLA, F-PLA, using a three-step process: (1) hydroxyl-terminated PLA was synthesized through the ROP of L-lactide; (2) the hydroxyl end group of PLA was blocked with Boc-L-phenylalanine; and (3) the free amino end group was obtained by removal of the *t*-butoxycarbonyl group. The resulting F-PLA conjugate was employed as macroinitiator for the synthesis of poly(L-lactide)-*b*-poly(L-lysine) block copolymers.

We prepared and characterized F-PLA and FF-PLA using an alternative process [87] to the one discussed above [88]. Accordingly, the polymer was grown from the peptide segment, which was used as initiator of the polymerization reaction (Fig. 6a). This conjugate exhibited relatively high molecular weights (i.e., 49,000 and 66,000 g/mol and

polydispersity of 1.41 and 1.48 for F-PLA and FF-PLA, respectively) and a yield of ~70 % for the PLA component. A suitable choice of the reaction time and temperature avoided thermal degradation of the biomaterial. The degree of crystallinity was around 30–33 % for the two hybrids, which is consistent with the relatively long segments arranged in a 10_7 helical conformation identified by FTIR spectroscopy. Circular dichroism (CD) spectroscopy was used to examine the possible interactions between the peptide and polymer fragments in the conjugates, with the results indicating the absence of interaction between the two fragments for F-PLA and very weak for FF-PLA.

To gain microscopic information about the level organization of the fragments and the level of interaction among them, MD simulations were performed on a model conjugate formed by a 40 residues-long tail of PLA linked to the C-terminus of a diphenylalanine peptide. Simulations, which were performed in 1,1,1,3,3,3-hexafluuoroisopropanol to facilitate the comparison with available experimental data, evidenced that the peptide fragment retains the intrinsic conformational preferences of diphenylalanine. This conclusion was in agreement with the relatively scarce interactions found between the FF and PLA blocks by CD spectroscopy. Indeed, the existent interactions were restricted to hydrogen bonds between the nonterminal phenylalanine residue and the L-lactide unit immediately after it. Thus, PLA tends to organize independently, which is essential for the construction of peptide guided assemblies.

Similar conclusions were reached in a previous study devoted to the hybrid amphiphile formed by the conjugation of a hydrophobic peptide with four phenylalanine (Phe) residues and hydrophilic poly(ethylene glycol) (PEG), hereafter denoted FFFF-PEG. This polymer is widely used in biomedicine because its properties as steric stabilizer, which help to encapsulate insoluble small molecules such as drugs, prevent or hinder their uptake, and facilitate their slow release. Experimental results reported by Castelletto and Hamley [89] revealed that FFFF-PEG tends to aggregate via hydrophobic interactions, even at moderately low concentrations, with a characteristic critical aggregation concentration. Above it, β-sheet organizations are detectable even before straight fibril structures start growing and depositing. These aggregates are much shorter than those observed for amyloid peptides though. Finally, PEG crystallization does not disrupt local β-sheet structure, even though on longer length scales the β-sheet fibrillar structure might be perturbed by the formation of spherulites from PEG crystallization. Theoretical studies using a combination of quantum mechanical calculations and atomistic molecular dynamics simulations allowed us to conclude that the two counterparts of FFFF-PEG amphiphile tend to organize as independent modules [90], as was also proved for FF-PLA.

Recently our lab has developed a new strategy for the preparation of peptide-polymer conjugates. This approach is based on the concept of chemical similarity of the two components of the conjugate. In order to achieve this similarity, exotic amino acids bearing the chemical characteristics of the polymer are designed and, subsequently, synthesized (e.g., Fig. 6). For example, synthetic amino acids bearing a 3,4-ethylenedioxythiophene (EDOT) were prepared to produce conjugates with poly(3,4-ethylenedioxithiophene) [91, 92], abbreviated PEDOT. The latter is among the most successful electroactive conducting polymers due to its excellent electrochemical and thermal properties, high conductivity,

good environmental stability in its doped state, mechanical flexibility, relative ease of preparation, and fast doping-undoping process [93, 94]. We showed that the conjugates obtained by linking such synthetic amino acids with PEDOT (named PEDOT-I and PEDOT-II in Scheme 1) exhibit electrochemical and electrical activity. Furthermore, cell adhesion and proliferation assays showed that the behavior of both PEDOT-I and PEDOT-II as cellular matrices is better than is PEDOT counterpart, the latter being a well-known electro-biocompatible material [91, 95].

Inspired by such results, we have recently used the strategy based on chemical similarity to design an electroactive Arg-Gly-Asp (RGD)-based peptide-PEDOT conjugate. For this purpose, the Gly residue of the RGD sequence has been replaced by amino acids bearing a 3,4-ethylenedioxythiophene as a side group [96]. The resulting sequence, hereafter denoted $RG^{E}D$ has been attached to the end of PEDOT chains forming the PEDOT-$RG^{E}D$ conjugate (Fig. 6b). This conjugate, which has been found to combine the cell adhesive activity of the RGD sequence with the electrochemical activity of PEDOT, behaves as an excellent soft bioelectroactive support for tissue regeneration through electrostimulation.

From a theoretical point of view, studies on PEDOT-I, PEDOT-II and PEDOT-$RG^{E}D$ pointed that they differ from FF-PLA and FFFF-PEG. PEDOT is a relatively rigid polymer and the most relevant properties of the electroactive conjugates refer to electron delocalization and electronic transitions. The conformational flexibility of the amino acids and the $RG^{E}D$ peptide were examined using quantum mechanical methods [92, 96]. The most stable conformers were coupled to a small PEDOT chain and the electronic properties in different environments were predicted using methods such as time-dependent density functional theory, and TD-DFT calculations to rationalize experimental observations.

3.1 Amyloid Peptides

Amyloid peptides, regardless of their sizes, functions, and sequences, have great potential as building blocks in the creation of dysfunctional/functional nanostructures, because they have natural ability to self-assemble into nanofibrillar structures and can be easily modified with various functional groups. Under the disease conditions, amyloid peptides can misfold and self-assemble into different dysfunctional nanostructures at the intermediate and final aggregation stages including linear, micelles, and annular organizations [97–99]. These dysfunctional amyloid nanostructures are known to be associated with more than 20 neurodegenerative diseases, including Alzheimer’s, Parkinson’s, Huntington’s, type II diabetes, and prion diseases [100–103]. Dysfunctional amyloid nanostructures adopt different structural morphologies, but they all contain certain degrees of cross-β-sheet structures, suggesting that amyloid oligomerization/fibrillization proceeds through different assembly pathways [104]. On the other hand, amyloid peptides can also form functional nanostructures, which help to regulate biological functions in synapse formation [105], hormone reservoir manufacture [84], and antimicrobial properties [106, 107]. Amyloid fibrils as final aggregation products of different amyloid peptides are robust, with mechanical strength similar to spider silk [108] and structural stability similar to barnacle cement [109]. Amyloid fibrils are also highly resistant to degradation and damage by proteases [110], UV light exposure [111], and high temperature of water [112, 113]. Thus

amyloid fibers have been functionalized for applications in metal nanowires [114–116], tissue engineering [117, 118], and drugand gene delivery [119, 120].

Both dysfunctional and functional amyloid nanostructures are biologically important for different applications. Thus, obtaining atomic-level structures of amyloid aggregates is an important step towards not only understanding amyloid functions and its underlying aggregation principles, but also structural-based design of functional amyloids. Different experimental techniques are used to probe structural information and biological function of amyloidosis. Solid-state NMR and X-ray diffraction are good approaches for resolving atomic-level structural information [78, 121, 122], but the nature of protein aggregation (noncrystallization and insolubility of fibrils, small sizes, short-lived states, involvement of cell membrane) renders these experimental studies extremely challenging [123, 124]. AFM and EM techniques can provide morphological images at nanoscale [125–127], but detailed structural and kinetic information are not reliable, even though EM is now approaching atomic scale resolution. The difficulties and limitations of these experimental methods in structural determination have inspired intensive computational studies to complement experiments. Most computer simulations of amyloid-forming peptides fall into two levels, atomic and coarse-grained with explicit and implicit solvent models [128]. All-atom molecular dynamics (MD) simulations have been applied to study relatively small amyloid oligomers by testing different candidate β-sheet arrangements of preformed oligomers mimicking possible nucleus seeds at the very early stage of amyloid formation [72, 129–131]. This approach can determine the most stable conformation for minimal nucleus seeds at the lowest free energy state, but cannot provide the aggregation scenario of amyloid intermediates/fibril growth since aggregation is an extremely slow process on the timescale of minutes to days, which is typically beyond the timescale of nanoseconds for conventional MD simulations. To overcome computational limitations, alternative computer simulations using low-resolution models (e.g., coarse-grained protein models and implicit solvent models) have been used to directly study the formation of oligomers (small species) and even fibrils (large species) [123, 132]. These simulations can qualitatively provide information on the kinetic pathways of protein aggregation, but cannot adequately capture different detailed interactions, such as hydrophobic interactions, electrostatic interactions, and hydrogen bonding. Once the amyloid structures are determined, structure-based design of functional amyloids becomes achievable. Experimental and theoretical methods have strengths and weaknesses, but a combination of experimental, theoretical, and computational methods can capture amyloid nanostructures at different length and time scales.

3.1.1 General Protocol—From a computational point of view, amyloid oligomers should be (meta)stable in solution so that they do have enough time to interact with the cell membrane and impair the cells by either forming specific-ion-leakage channel or thinning/damaging cell membrane. If the oligomers are unstable, they quickly disassociate into monomers or aggregate into mature fibrils, which have been shown to have less damage to cells. Thus, identification of stable oligomers that are able to retain their initial structural organization at the lowest free energy state in simulations is the first step to correlate amyloid structures with their biological functions. In this section, we present a general computational protocol of our peptide-packing program, which is used to predict atomic

structures of amyloid fibrils/oligomers. Figure 7 depicts the overview of the protocol workflow of the peptide packing program, consisting of the following steps:

1. Rigid-body packing.: The rigid-body packing module is used for "coarse" structural prediction: (a) The building block can be either amyloid monomer or oligomer. (b) The assembly symmetry should be given. (c) The key peptide-peptide reaction coordinates should be predefined. For a twofold symmetry, the displacement and orientation of one β-sheet with respect to the other are key coordinates; for a threefold symmetry, the rotation of β-sheet with respect to the others is a key coordinate, and for a spherical symmetry, peptide self-rotation, peptide-to-peptide displacement and orientation, and layer-to-layer orientation are key coordinates. (d) The distance between β-sheets should be set to 10 Å, which corresponds to the average distance in a cross-β structure; the distance between β-strands should be 4.7 Å, which allows chains to form hydrogen bonds. (e) A local energy minimization is used to remove any steric clash. (f) Hydrophobic contacts, hydrogen bonding, shape-complementary parameters are calculated and used as criteria to tune rigid-body movement for optimizing backbone-backbone and side chain–side chain interactions.

2. Structural refinement.: Peptide flexibility presents a major challenge in molecular docking and assembly [133], because peptide flexibility, including backbone and side chain movements significantly extends the search space for optimal structure of the assembly. In this module, a Monte Carlo Minimization (MCM) method will be used to handle backbone and side chain flexibility. Each MCM cycle consists of (a) rigid body perturbation (i.e., peptide translation and peptide rotation), (b) backbone and side chain optimization (i.e., torsion angle rotation), and (c) steepest descent minimization.

3. Molecular mechanic generalized-born surface area (MM-GBSA).: The MM-GBSW method has been implemented in the peptide packing program and used to score and rank all peptide assemblies in terms of free energy. The MM-GBSA approach, combined the molecular mechanics with the implicit solvent generalized-born method and CHARMM force field [68, 134] can accurately reproduce the folding and assembly of membrane proteins in aqueous solution and in heterogeneous biological membranes [135], but is much less computationally demanding due to the largely reduced number of degrees of freedom. The free energy of the system (G) is computed by $G = G_{polar} + G_{nonpolar} + E_{mm} - TS$, where a polar solvation energy (G_{polar}) is computed by the GB model; a nonpolar solvation energy ($G_{nonpolar}$) is computed from a solvent-accessible surface area model; a molecular mechanics energy (E_{mm}) is a sum of bonds, angles, torsions, van der Waals, and electrostatic interactions; and the entropy effect by solute vibration is estimated by the normal mode calculation.

4. Explicit-solvent molecular dynamics (MD) simulations.: Once amyloid nanostructured aggregates are obtained from **steps 1–3**, they are subject to solvent explicit-solvent MD simulations to validate their structural stability. In general, amyloid aggregates are solvated in a TIP3P water cubic box with a margin of at least 15 Å from any edge of the water box to any peptide atom. Water molecules within 2.4 Å of the amyloid aggregates are removed to avoid initial overlapping. The systems are then neutralized by adding counter

ions of Cl^- and Na^+ to reach ionic strength of interest (i.e., 100 ~ 150 mM). The resulting systems are minimized in energy for 5000 steps with peptides restrained, followed by additional 5000 steps of minimization for the whole system to remove unfavorable contacts between solvent and peptides. Next, the systems are subject to 1 ns MD run with harmonica constrained on the backbone atoms of the peptides. The production runs are carried out in the NPT ensemble (i.e., 1 atm and 300 K). Constant pressure and temperature in the system are maintained by an isotropic Langevin barostat and a Langevin thermostat, respectively. Long-range electrostatics interactions are treated by the particle mesh Ewald sum method, while short-range van der Waals (VDW) interactions are typically evaluated by a switching method with a twin range cutoff of 10 and 12 Å. The integration time step is 2 fs with the RATTLE algorithm applied to constrain bonds involving hydrogen atoms. Periodic boundary condition with the minimum image convention is applied to all directions. All models are run twice to validate simulation convergence by using the same starting coordinates but different initial velocities assigned by the Maxwell-Boltzman distribution. In our studies, all MD simulations are performed by the NAMD program [67] with all-atom CHARMM27 force field [134].

3.1.2 Representative Example of Aβ Micelles—We have used the peptide packing program, combined with structural information available from experiments, to determine a series of atomic structures of amyloid-β (Aβ) linears [136, 137], micelles [138], triangulars [139], snowflakes [140], annulars [141], and globulomers [142] (Fig. 8), hIAPP stacking-sandwich oligomers [143] and wrapping-cord triangular oligomers [144], and Tau octamers with three- and four-repeat segments [145–147]. These oligomers vary considerably in β-sheet packing and orientation, but all display high structural stability, reflecting a highly polymorphic nature of amyloids in a rugged energy landscape along different aggregation pathways. In addition, structural analysis also reveals that different β-sheet associations provide different driving forces to stabilize intra-sheet organization via Asn/Gln ladders, aromatic stacking, and continuous hydrogen bonding.

Here we presented a protocol to construct more complex Aβ micelles as an example. Figure 9 shows a three-step procedure to build a micelle. First, single $A\beta_{25–35}$ peptide was aligned to the *z* axis with a minimal distance of ~4 Å from the origin of the Cartesian coordinate. Second, the peptide was replicated and rotated along the *y* axis at every 30° to form a semi-circle by seven A, B, C, D, E, F, G peptides with the same parallel orientation in the *xz* plane. Then, peptides of B, D, and F are rotated additional 15 along the *z* axis so that peptides of A, C, E, and G and peptides of B, D, and F are located in different planes. For the antiparallel packing, peptides of A, C, E, and G were reversed to impose opposite orientation relative to peptides of B, D, and F. Finally, five peptides of B, C, D, E, and F (exclusion of A and G) were rotated and copied along the *z* axis at every 30° to form a micelle consisting of different circle layers, namely B, C, D, E, and F layers. Each layer consists of 12 peptides except A and G layers, leading to total 62 peptides in the micelle. Four micelle structures were subject to “coarse” structure optimization by using energy minimization with generalized born of a simple switching function (GBSW) implicit solvent model [148]. For each “coarse-optimized” micelle, we further refined the structure by adjusting peptide self-rotating angle (Φ) along the helical axis and peptide displacement

between different layers (λ), i.e., each peptide was rotated along its helical axis at every 15° to avoid side-chain clash, while peptides of A, C, E, and G were moved with respect to peptides of B, D, F along the opposite direction. The structure-refining procedure generated 504 distinct structures for each “coarse-optimized” micelle. A total of 2016 micelles were energy-minimized by using 300 steps of steepest decent with backbone constrained, followed by 200 steps conjugate and 300 steps steep decent minimization without position constrains in the presence of the GBSW implicit solvent. Four different lowest-energy micelles, one from each category (i.e., parallel or antiparallel orientations with N- or C-terminal exposed to solvent)), were selected and subject to explicit-solvent MD simulation for examining their structural and energetic aspects at the early stage of aggregation process. Collective MD simulations identified the Aβ micelles with antiparallel orientations as not only with high structural stability, but also high binding affinity to an antibody, suggesting that these Aβ micelles may present more biologically relevant species.

Acknowledgements

J.Z. thanks for financial supports from the National Science Foundation (CAREER Award 0952624, 1510099, and 1607475) and Alzheimer Association—New Investigator Research Grant (2015-NIRG-341372), and National Natural Science Foundation of China (NSFC-21528601). The calculations were carried out in part on the UMass Boston research cluster. This work has been funded in whole or in part with Federal funds from the National Cancer Institute, National Institutes of Health, under contract number HHSN261200800001E. The content of this publication does not necessarily reflect the views or policies of the Department of Health and Human Services, nor does mention of trade names, commercial products, or organizations imply endorsement by the U.S. Government. This research was supported (in part) by the Intramural Research Program of the NIH, National Cancer Institute, Center for Cancer Research.

References

1. Ferrari M (2005) Cancer nanotechnology: opportunities and challenges. Nat Rev Cancer 5(3):161–171 [PubMed: 15738981]
2. Ferrari M (2005) Nanovector therapeutics. Curr Opin Chem Biol 9(4):343–346 [PubMed: 15967706]
3. Blanco E et al. (2011) Nanomedicine in cancertherapy: innovative trends and prospects. Cancer Sci 102(7):1247–1252 [PubMed: 21447010]
4. Gradišar H, Jerala R (2014) Self-assembled bionanostructures: proteins following the lead of DNA nanostructures. J Nanobiotechnol 12:4
5. Rubin DJ et al. (2015) Structural, nanomechanical, and computational characterization of d,l-cyclic peptide assemblies. ACS Nano 9 (3):3360–3368 [PubMed: 25757883]
6. Balzani V, Credi A, Venturi M (2009) Lightpowered molecular machines. Chem Soc Rev 38(6):1542–1550 [PubMed: 19587950]
7. King NP et al. (2012) Computational design of self-assembling protein nanomaterials with atomic level accuracy. Science 336 (6085):1171–1174 [PubMed: 22654060]
8. Zhang Z-J et al. (2013) A double-leg donor–acceptor molecular elevator: new insight into controlling the distance of two platforms. Org Lett 15(7):1698–1701 [PubMed: 23534551]
9. Pei H et al. (2014) Functional DNA nanostructures for theranostic applications. Acc Chem Res 47(2):550–559 [PubMed: 24380626]
10. Rangnekar A, LaBean TH (2014) Building DNA nanostructures for molecular computation, templated assembly, and biological applications. Acc Chem Res 47(6):1778–1788 [PubMed: 24720350]
11. Bindewald E et al. (2008) RNAJunction: a database of RNA junctions and kissing loops for three-dimensional structural analysis and nanodesign. Nucleic Acids Res 36(database issue):D392–D397 [PubMed: 17947325]

12. Mathur D, Henderson ER (2013) Complex DNA nanostructures from oligonucleotide ensembles. ACS Synth Biol 2(4):180–185 [PubMed: 23656476]
13. Li H, LaBean TH, Leong KW (2011) Nucleic acid-based nanoengineering: novel structures for biomedical applications. Interface Focus 1 (5):702–724 [PubMed: 23050076]
14. Grabow WW et al. (2011) Self-assembling RNA nanorings based on RNAI/II inverse kissing complexes. Nano Lett 11(2):878–887 [PubMed: 21229999]
15. Miller BG, Raines RT (2005) Reconstitution of a defunct glycolytic pathway via recruitment of ambiguous sugar kinases†. Biochemistry 44(32):10776–10783 [PubMed: 16086580]
16. Bang D, Kent SBH (2005) His(6) tag-assisted chemical protein synthesis. Proc Natl Acad Sci U S A 102(14):5014–5019 [PubMed: 15784744]
17. Miller Y, Ma B, Nussinov R (2015) Polymorphism in self-assembly of peptide-based β-hairpin contributes to network morphology and hydrogel mechanical rigidity. J Phys Chem B 119(2):482–490 [PubMed: 25545881]
18. Tsai H-H et al. (2004) In silico protein design by combinatorial assembly of protein building blocks. Protein Sci 13(10):2753–2765 [PubMed: 15388863]
19. Main ERG et al. (2005) A recurring theme in protein engineering: the design, stability and folding of repeat proteins. Curr Opin Struct Biol 15(4):464–471 [PubMed: 16043339]
20. Jenkins J, Mayans O, Pickersgill R (1998) Structure and evolution of parallel [beta]-helix proteins. J Struct Biol 122 (1–2):236–246 [PubMed: 9724625]
21. Haspel N et al. (2006) De novo tubular nanostructure design based on self-assembly of [beta]-helical protein motifs. Structure 14 (7):1137–1148 [PubMed: 16843895]
22. Bernstein FC, The protein data bank et al.(1977) Eur J Biochem 80(2):319–324 [PubMed: 923582]
23. Haspel N et al. (2007) Changing the charge distribution of {beta}-helical-based nanostructures can provide the conditions for charge transfer. Biophys J 93(1):245–253 [PubMed: 17416628]
24. Schmitz K (2010) Amino acids, peptides and proteins in organic chemistry. Volume 1–Origins and synthesis of amino acids. Edited by Hughes Andrew B.. Angew Chem Int Ed 49 (22):3717–3718
25. Vadim AS, Kunisuke I (2009) Asymmetric synthesis and application of α-amino acids In: ACS symposium series, vol 1009 American Chemical Society, p. 512.
26. Christophorou MA et al. (2014) Citrullination regulates pluripotency and histone H1 binding to chromatin. Nature 507 (7490):104–108 [PubMed: 24463520]
27. Cativiela C, Ordonez M (2009) Recent progress on the stereoselective synthesis of cyclic quaternary alpha-amino acids. Tetrahedron Asymmetry 20(1):1–63 [PubMed: 20300486]
28. Michaux J, Niel G, Campagne JM (2009) Stereocontrolled routes to beta, beta′-disub-stituted alpha-amino acids. Chem Soc Rev 38 (7):2093–2116 [PubMed: 19551183]
29. Degenkolb T, Bruckner H (2008) Peptaibiomics: towards a myriad of bioactive peptides containing C(alpha)-dialkylamino acids? Chem Biodivers 5(9):1817–1843 [PubMed: 18816513]
30. Schwarzer D, Finking R, Marahiel MA (2003) Nonribosomal peptides: from genes to products. Nat Prod Rep 20(3):275–287 [PubMed: 12828367]
31. Nestor JJ Jr (2009) The medicinal chemistry of peptides. Curr Med Chem 16(33):4399–4418 [PubMed: 19835565]
32. Horne WS, Gellman SH (2008) Foldamers with heterogeneous backbones. Acc Chem Res 41(10):1399–1408 [PubMed: 18590282]
33. Ersmark K, Del Valle JR, Hanessian S (2008) Chemistry and biology of the aeruginosin family of serine protease inhibitors. Angew Chem Int Ed Engl 47(7):1202–1223 [PubMed: 18076006]
34. Voloshchuk N, Montclare JK (2010) Incorporation of unnatural amino acids for synthetic biology. Mol Biosyst 6(1):65–80 [PubMed: 20024068]
35. Wu X, Schultz PG (2009) Synthesis at the interface of chemistry and biology. J Am Chem Soc 131(35):12497–12515 [PubMed: 19689159]
36. Murakami H et al. (2000) Site-directed incorporation of fluorescent nonnatural amino acids into streptavidin for highly sensitive detection of biotin. Biomacromolecules 1 (1):118–125 [PubMed: 11709833]

37. Vazquez ME et al. (2003) Fluorescent caged phosphoserine peptides as probes to investigate phosphorylation-dependent protein associations. J Am Chem Soc 125 (34):10150–10151 [PubMed: 12926919]
38. Alfonta L et al. (2003) Site-specific incorporation of a redox-active amino acid into proteins. J Am Chem Soc 125(48):14662–14663 [PubMed: 14640614]
39. Lemke EA et al. (2007) Control of protein phosphorylation with a genetically encoded photocaged amino acid. Nat Chem Biol 3 (12):769–772 [PubMed: 17965709]
40. Wang W et al. (2007) Genetically encoding unnatural amino acids for cellular and neuronal studies. Nat Neurosci 10(8):1063–1072 [PubMed: 17603477]
41. Cellitti SE et al. (2008) In vivo incorporation of unnatural amino acids to probe structure, dynamics, and ligand binding in a large protein by nuclear magnetic resonance spectroscopy. J Am Chem Soc 130(29):9268–9281 [PubMed: 18576636]
42. Summerer D et al. (2006) A genetically encoded fluorescent amino acid. Proc Natl Acad Sci U S A 103(26):9785–9789 [PubMed: 16785423]
43. Lee HS et al. (2009) Genetic incorporation of a small, environmentally sensitive, fluorescent probe into proteins in Saccharomyces cerevisiae. J Am Chem Soc 131(36):12921–12923 [PubMed: 19702307]
44. Zanuy D et al. (2007) Use of constrained synthetic amino acids in beta-helix proteins for conformational control. J Phys Chem B 111 (12):3236–3242 [PubMed: 17388467]
45. Zanuy D et al. (2009) Protein segments with conformationally restricted amino acids can control supramolecular organization at the nanoscale. J Chem Inf Model 49 (7):1623–1629 [PubMed: 19548653]
46. Tu RS, Tirrell M (2004) Bottom-up design of biomimetic assemblies. Adv Drug Deliv Rev 56(11):1537–1563 [PubMed: 15350288]
47. Lee MR et al. (2009) Nylon-3 copolymers that generate cell-adhesive surfaces identified by library screening. J Am Chem Soc 131 (46):16779–16789 [PubMed: 19886604]
48. Revilla-Lopez G et al. (2010) NCAD, a database integrating the intrinsic conformational preferences of non-coded amino acids. J Phys Chem B 114(21):7413–7422 [PubMed: 20455555]
49. Aleman C (1997) Conformational properties of [alpha]-amino acids disubstituted at the [alpha]-carbon. J Phys Chem B 101 (25):5046–5050
50. Alemán C, Casanovas J, Galembeck SE (1998) PAPQMD parametrization of molecular systems with cyclopropyl rings: conformational study of homopeptides constituted by l-aminocyclopropane-l-carboxylic acid. J Computer-Aided Molecular Design 12 (3):259–273
51. Gomez-Catalan J, Aleman C, Perez JJ (2000) Conformational profile of 1-aminocyclopropanecarboxylic acid. Theor Chem Acc 103(5):380–389
52. Benedetti E et al. (1989) Structural versatility of peptides containing C-alpha, alpha-dialkylated glycines. An X-ray diffraction study of 6 1-aminocyclopropane-1-carboxylic acid rich peptides. Int J Biol Macromol 11 (6):353–360 [PubMed: 2489104]
53. Benedetti E et al. (1989) Structural versatility of peptides from C[alpha, alpha] dialkylated glycines: linear Ac3c homo-oligopeptides. Biopolymers 28(1):175–184
54. Fabiano N et al. (1993) Conformational versatility of the N-alpha-acylated tripeptide amide tail of oxytocin - synthesis and crystallographic characterization of 3C-2-alpha-backbone modified, conformationally restricted analogs. Int J Pept Protein Res 42 (5):459–465 [PubMed: 8106198]
55. Valle G et al. (1989) Linear oligopeptides. 200. crystallographic characterization of conformation of 1-aminocyclopropane-1-carboxylic acid residue (Ac3c) in simple derivatives and peptides. Int J Pept Protein Res 34 (1):56–65 [PubMed: 2793309]
56. Aleman C et al. (2002) Influence of the phenylside chain on the conformation of cyclopropane analogues of phenylalanine. J Phys Chem B 106(45):11849–11858
57. Toniolo C et al. (2001) Control of peptide conformation by the Thorpe-Ingold effect (C-alpha-tetrasubstitution). Biopolymers 60 (6):396–419 [PubMed: 12209474]
58. Hruby VJ et al. (1997) Design of peptides, proteins, and peptidomimetics in chi space. Biopolymers 43(3):219–266 [PubMed: 9277134]

59. Jimenez AI, Cativiela C, Marraud M (2000) Agamma-turn induced by a highly constrained cyclopropane analogue of phenylalanine (c(3) diPhe) in the solid state. Tetrahedron Lett 41 (28):5353–5356
60. Jimenez AI et al. (1998) Beta-turn preferences induced by 2,3-methanophenylalanine chirality. J Am Chem Soc 120(37):9452–9459
61. Jimenez AI et al. (1997) Folding types of dipeptides containing the diastereoisomeric cyclopropanic analogues of phenylalanine. Tetrahedron Lett 38(43):7559–7562
62. Casanovas J et al. (2003) N-Acetyl-N′-methylamide derivative of (2S,3S)-1-amino-2,3diphenylcyclopropanecarboxylic acid: theoretical analysis of the conformational impact produced by the incorporation of the second phenyl group to the cyclopropane analogue of phenylalanine. J Org Chem 68 (18):7088–7091 [PubMed: 12946154]
63. Jiménez AI, Ballano G, Cativiela C (2005) First observation of two consecutive gamma turns in a crystalline linear dipeptide. Angew Chem Int Ed 44(3):396–399
64. Casanovas J et al. (2006) Conformational analysis of a cyclopropane analogue of phenylalanine with two geminal phenyl substituents. J Phys Chem B 110(11):5762–5766 [PubMed: 16539522]
65. Crisma M et al. (2006) Preferred 3D-structure of peptides rich in a severely conformationally restricted cyclopropane analogue of phenylalanine. Chemistry 12(1):251–260
66. Royo S et al. (2005) Turn and helical peptide handedness governed exclusively by side-chain chiral centers. J Am Chem Soc 127 (7):2036–2037 [PubMed: 15713068]
67. Kale L et al. (1999) NAMD2: greater scalability for parallel molecular dynamics. J Comput Phys 151(1):283–312
68. MacKerell AD et al. (1998) All-atom empirical potential for molecular modeling and dynamics studies of proteins. J Phys Chem B 102 (18):3586–3616 [PubMed: 24889800]
69. William LJ et al. (1983) Comparison of simple potential functions for simulating liquid water. J Chem Phys 79(2):926–935
70. Darden T et al. (1999) New tricks for modelers from the crystallography toolkit: the particle mesh Ewald algorithm and its use in nucleic acid simulations. Structure 7(3): R55–R60 [PubMed: 10368306]
71. Haspel N et al. (2004) A comparative study of amyloid fibril formation by residues 15–19 of the human calcitonin hormone: a single beta-sheet model with a small hydrophobic core. J Mol Biol 345(5):1213–1227 [PubMed: 15644216]
72. Ma B, Nussinov R (2002) Stabilities and conformations of Alzheimer's beta-amyloid peptide oligomers (Abeta 16–22, Abeta 16–35, and Abeta 10–35): sequence effects. Proc Natl Acad Sci U S A 99(22):14126–14131 [PubMed: 12391326]
73. Ma B, Nussinov R (2002) Molecular dynamics simulations of alanine rich {beta}-sheet oligomers: insight into amyloid formation. Protein Sci 11(10):2335–2350 [PubMed: 12237456]
74. Ma B, Nussinov R (2003) Molecular dynamics simulations of the unfolding of {beta}2-microglobulin and its variants. Protein Eng 16(8):561–575 [PubMed: 12968074]
75. Zanuy D, Ma B, Nussinov R (2003) Short peptide amyloid organization: stabilities and conformations of the islet amyloid peptide NFGAIL. Biophys J 84(3):1884–1894 [PubMed: 12609890]
76. Zanuy D, Nussinov R (2003) The sequence dependence of fiber organization. A comparative molecular dynamics study of the islet amyloid polypeptide segments 22–27 and 22–29. J Mol Biol 329(3):565–584 [PubMed: 12767835]
77. Luhrs T et al. (2005) 3D structure of Alzheimer's amyloid-{beta}(1–42) fibrils. Proc Natl Acad Sci U S A 102(48):17342–17347 [PubMed: 16293696]
78. Petkova AT et al. (2002) A structural model for Alzheimer's beta-amyloid fibrils based on experimental constraints from solid state NMR. Proc Natl Acad Sci U S A 99 (26):16742–16747 [PubMed: 12481027]
79. Reches M, Porat Y, Gazit E (2002) Amyloid fibril formation by pentapeptide and tetrapeptide fragments of human calcitonin. J Biol Chem 277(38):35475–35480 [PubMed: 12095997]
80. Zanuy D et al. (2004) Peptide sequence and amyloid formation: molecular simulations and experimental study of a human islet amyloid polypeptide fragment and its analogs. Structure 12(3):439–455 [PubMed: 15016360]

81. Thompson JD, Gibson TJ, Higgins DG (2002) Multiple sequence alignment using ClustalW and ClustalX. Curr Protoc Bioinformatics Chapter 2:Unit 2.3.
82. Zhang S (2003) Fabrication of novel biomaterials through molecular self-assembly. Nat Biotechnol 21(10):1171–1178 [PubMed: 14520402]
83. Liu TY et al. (2013) Self-adjuvanting polymer-peptide conjugates as therapeutic vaccine candidates against cervical cancer. Biomacromolecules 14(8):2798–2806 [PubMed: 23837675]
84. Maji SK et al. (2009) Functional amyloids as natural storage of peptide hormones in pituitary secretory granules. Science 325 (5938):328–332 [PubMed: 19541956]
85. Vandermeulen GWM, Klok H-A (2004) Peptide/protein hybrid materials: enhanced control of structure and improved performance through conjugation of biological and synthetic polymers. Macromol Biosci 4 (4):383–398 [PubMed: 15468229]
86. Haspel N et al. (2012) Conformational exploration of two peptides and their hybrid polymer conjugates: potentialities as self-aggregating materials. J Phys Chem B 116 (48):13941–13952 [PubMed: 23157485]
87. Murase SK et al. (2014) Molecular characterization of l-phenylalanine terminated poly(l-lactide) conjugates. RSC Adv 4(44):23231–23241
88. Fan Y et al. (2005) l-Phe end-capped poly(l-lactide) as macroinitiator for the synthesis of poly(l-lactide)-b-poly(l-lysine) block copolymer. Biomacromolecules 6(6):3051–3056 [PubMed: 16283726]
89. Castelletto V, Hamley IW (2009) Self assembly of a model amphiphilic phenylalanine peptide/polyethylene glycol block copolymer in aqueous solution. Biophys Chem 141 (2–3):169–174 [PubMed: 19232813]
90. Zanuy D, Hamley IW, Aleman C (2011) Modeling the tetraphenylalanine-PEG hybrid amphiphile: from DFT calculations on the peptide to molecular dynamics simulations on the conjugate. J Phys Chem B 115 (28):8937–8946 [PubMed: 21671568]
91. Fabregat G et al. (2013) An electroactive and biologically responsive hybrid conjugate based on chemical similarity. Polym Chem 4 (5):1412–1424
92. Fabregat G et al. (2013) Design of hybrid conjugates based on chemical similarity. RSC Adv 3(43):21069–21083
93. Groenendaal L et al. (2003) Electrochemistry of poly(3,4-alkylenedioxythiophene) derivatives. Adv Mater 15(11):855–879
94. Kirchmeyer S, Reuter K (2005) Scientific importance, properties and growing applications of poly(3,4-ethylenedioxythiophene). J Mater Chem 15(21):2077–2088
95. Maione S et al. (2014) Electro-biocompatibility of conjugates designed by chemical similarity. J Pept Sci 20(7):537–546 [PubMed: 24902543]
96. Maione S, Gil A, Fabregat G, Del Valle LJ, Triguero J, Laurent A, Jacquemin D, Estrany F, Zanuy D, Cativiela C, Alemán C (2015) Electroactive polymer-peptide conjugates for adhesive biointerfaces. Biomater. Sci. (3):1395–1405. [PubMed: 26372182]
97. Gosal WS et al. (2005) Competing pathways determine fibril morphology in the self-assembly of [beta]2-microglobulin into amyloid. J Mol Biol 351(4):850–864 [PubMed: 16024039]
98. Lashuel HA et al. (2002) Amyloid pores from pathogenic mutations. Nature 418(6895):291
99. Lashuel HA et al. (2002) Alpha-synuclein, especially the parkinson's disease-associated mutants, forms pore-like annular and tubular Protofibrils. J Mol Biol 322(5):1089–1102 [PubMed: 12367530]
100. Dauer W, Przedborski S (2003) Parkinson's disease: mechanisms and models. Neuron 39 (6):889–909 [PubMed: 12971891]
101. Dobson CM (2005) Structural biology: prying into prions. Nature 435 (7043):747–749 [PubMed: 15944684]
102. Meredith SC (2006) Protein denaturation and aggregation: cellular responses to denatured and aggregated proteins. Ann N Y Acad Sci 1066(1):181–221
103. Selkoe DJ (2001) Alzheimer's disease: genes, proteins, and therapy. Physiol Rev 81 (2):741–766 [PubMed: 11274343]

104. Tycko R (2004) Progress towards a molecular-level structural understanding of amyloid fibrils. Curr Opin Struct Biol 14 (1):96–103 [PubMed: 15102455]
105. Si K et al. (2010) Aplysia CPEB can form prion-like multimers in sensory neurons that contribute to long-term facilitation. Cell 140 (3):421–435 [PubMed: 20144764]
106. Kagan BL, et al. (2011) Antimicrobial properties of amyloid peptides. Mol Pharm, Mol. Pharmaceutics, 2012, 9 (4):708–717
107. Zhang M, Zhao J, Zheng J (2014) Molecular understanding of a potential functional link between antimicrobial and amyloid peptides. Soft Matter 10(38):7425–7451 [PubMed: 25105988]
108. Slotta U et al. (2007) Spider silk and amyloid fibrils: a structural comparison. Macromol Biosci 7(2):183–188 [PubMed: 17295405]
109. Sullan RMA et al. (2009) Nanoscale structures and mechanics of barnacle cement. Biofouling 25(3):263–275 [PubMed: 19180351]
110. Ryu J, Park CB (2010) High stability of self-assembled peptide nanowires against thermal, chemical, and proteolytic attacks. Biotechnol Bioeng 105(2):221–230 [PubMed: 19777585]
111. Peralta MDR et al. (2015) Engineering amyloid fibrils from β-solenoid proteins for biomaterials applications. ACS Nano 9 (1):449–463 [PubMed: 25562726]
112. Arora A, Ha C, Park CB (2004) Insulin amyloid fibrillation at above 100C: new insights into protein folding under extreme temperatures. Protein Sci 13(9):2429–2436 [PubMed: 15295111]
113. Kardos J et al. (2011) Reversible heat-induced dissociation of β2-microglobulin amyloid fibrils. Biochemistry 50(15):3211–3220 [PubMed: 21388222]
114. Reches M, Gazit E (2003) Casting metal nanowires within discrete self-assembled peptide nanotubes. Science 300(5619):625–627 [PubMed: 12714741]
115. Sakai H et al. (2013) Formation of functionalized nanowires by control of self-assembly using multiple modified amyloid peptides. Adv Funct Mater 23(39):4881–4887
116. Scheibel T et al. (2003) Conducting nanowires built by controlled self-assembly of amyloid fibers and selective metal deposition. Proc Natl Acad Sci U S A 100(8):4527–4532 [PubMed: 12672964]
117. Gras SL et al. (2008) Functionalised amyloid fibrils for roles in cell adhesion. Biomaterials 29(11):1553–1562 [PubMed: 18164758]
118. Holmes TC et al. (2000) Extensive neurite outgrowth and active synapse formation on self-assembling peptide scaffolds. Proc Natl Acad Sci U S A 97(12):6728–6733 [PubMed: 10841570]
119. Koutsopoulos S et al. (2009) Controlled release of functional proteins through designer self-assembling peptide nanofiber hydrogel scaffold. Proc Natl Acad Sci U S A 106(12):4623–4628 [PubMed: 19273853]
120. Li D et al. (2014) Structure-based design of functional amyloid materials. J Am Chem Soc 136(52):18044–18051 [PubMed: 25474758]
121. Chamberlain AK et al. (2001) Characterization of the structure and dynamics of amyloidogenic variants of human lysozyme by NMR spectroscopy. Protein Sci 10(12):2525–2530 [PubMed: 11714920]
122. Tycko R (2000) Solid-state NMR as a probe of amyloid fibril structure. Curr Opin Chem Biol 4(5):500–506 [PubMed: 11006536]
123. Mousseau N, Derreumaux P (2005) Exploring the early steps of amyloid peptide aggregation by computers. Acc Chem Res 38(11):885–891 [PubMed: 16285711]
124. Makabe K et al. (2006) Atomic structures of peptide self-assembly mimics. Proc Natl Acad Sci U S A 103(47):17753–17758 [PubMed: 17093048]
125. Benseny-Cases N, Cocera M, Cladera J (2007) Conversion of non-fibrillar [beta]-sheet oligomers into amyloid fibrils in Alzheimer's disease amyloid peptide aggregation. Biochem Biophys Res Commun 361 (4):916–921 [PubMed: 17679138]
126. Legleiter J et al. (2004) Effect of different anti-A[beta] antibodies on a[beta] fibrillogenesis as assessed by atomic force microscopy. J Mol Biol 335(4):997–1006 [PubMed: 14698294]
127. Wang Z et al. (2003) AFM and STM study of [beta]-amyloid aggregation on graphite. Ultramicroscopy 97(1–4):73–79 [PubMed: 12801659]

128. Morriss-Andrews A, Shea J-E (2014) Simulations of protein aggregation: insights from atomistic and coarse-grained models. J Phys Chem Lett 5(11):1899–1908 [PubMed: 26273871]
129. Tsai H-H et al. (2005) Energy landscape of amyloidogenic peptide oligomerization by parallel-tempering molecular dynamics simulation: significant role of Asn ladder. Proc Natl Acad Sci U S A 102(23):8174–8179 [PubMed: 15923262]
130. Zheng J et al. (2006) Structural stability and dynamics of an amyloid-forming peptide GNNQQNY from the yeast prion sup-35. Biophys J 91(3):824–833 [PubMed: 16679374]
131. Zheng J et al. (2007) Nanostructure design using protein building blocks enhanced by conformationally constrained synthetic residues. Biochemistry 46(5):1205–1218 [PubMed: 17260950]
132. Nguyen HD, Hall CK (2006) Spontaneous fibril formation by polyalanines: discontinuous molecular dynamics simulations. J Am Chem Soc 128(6):1890–1901 [PubMed: 16464090]
133. Andrusier N et al. (2008) Principles of flexible protein-protein docking. Proteins 73 (2):271–289 [PubMed: 18655061]
134. Brooks BR et al. (1983) CHARMM: a program for macromolecular energy, minimization, and dynamics calculations. J Comput Chem 4(2):187–217
135. Im W, Feig M, Brooks CL III (2003) An implicit membrane generalized born theory for the study of structure, stability, and interactions of membrane proteins. Biophys J 85 (5):2900–2918 [PubMed: 14581194]
136. Wang Q et al. (2011) Structural, morphological, and kinetic studies of beta-amyloid peptide aggregation on self-assembled monolayers. Phys Chem Chem Phys 13 (33):15200–15210 [PubMed: 21769359]
137. Yu X et al. (2010) Atomic-scale simulations confirm that soluble [beta]-sheet-rich peptide self-assemblies provide amyloid mimics presenting similar conformational properties. Biophys J 98(1):27–36 [PubMed: 20085717]
138. Yu X, Wang Q, Zheng J (2010) Structural determination of A[beta]25–35 micelles by molecular dynamics simulations. Biophys J 99(2):666–674 [PubMed: 20643087]
139. Zheng J et al. (2010) Molecular modeling of two distinct triangular oligomers in amyloid beta-protein. J Phys Chem B 114(1):463–470 [PubMed: 20014755]
140. Li L, Zheng J (2010) Computational modeling of amyloid oligomeric structures. Inter J Liquid State Sci 1(1):1–13
141. Zheng J et al. (2008) Annular structures as intermediates in fibril formation of Alzheimer A[beta]17–42. J Phys Chem B 112 (22):6856–6865 [PubMed: 18457440]
142. Yu X, Zheng J (2011) Polymorphic structures of Alzheimer's β-amyloid globulomers. PLoS One 6(6):e20575 [PubMed: 21687730]
143. Zhao J et al. (2011) Structural polymorphism of human islet amyloid polypeptide (hIAPP) oligomers highlights the importance of interfacial residue interactions. Biomacromolecules 12(1):210–220 [PubMed: 21158384]
144. Zhao J et al. (2011) Heterogeneous triangular structures of human islet amyloid polypeptide (amylin) with internal hydrophobic cavity and external wrapping morphology reveal the polymorphic nature of amyloid fibrils. Biomacromolecules 12(5):1781–1794 [PubMed: 21428404]
145. Luo Yet al. (2013) Molecular insights into the reversible formation of tau protein fibrils. Chem Commun 49(34):3582–3584
146. Siddiqua A et al. (2012) Conformational basisfor asymmetric seeding barrier in filaments of three- and four-repeat tau. J Am Chem Soc 134(24):10271–10278 [PubMed: 22656332]
147. Yu X et al. (2012) Cross-seeding and conformational selection between three- and four-repeat human Tau proteins. J Biol Chem 287 (18):14950–14959 [PubMed: 22393063]
148. Im W, Lee MS, Brooks CL III (2003) Generalized born model with a simple smoothing function. J Comput Chem 24 (14):1691–1702 [PubMed: 12964188]

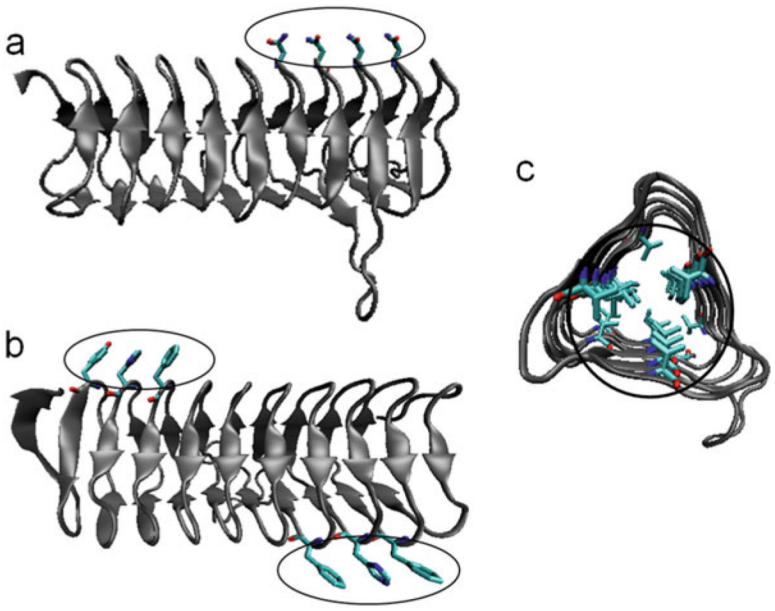

Fig. 1.

An example of β-helical proteins and their typical interactions. (**a**) An example of an asparagine ladder. (**b**) An example of aromatic ring stacking. (**c**) An example of hydrophobic residue interactions

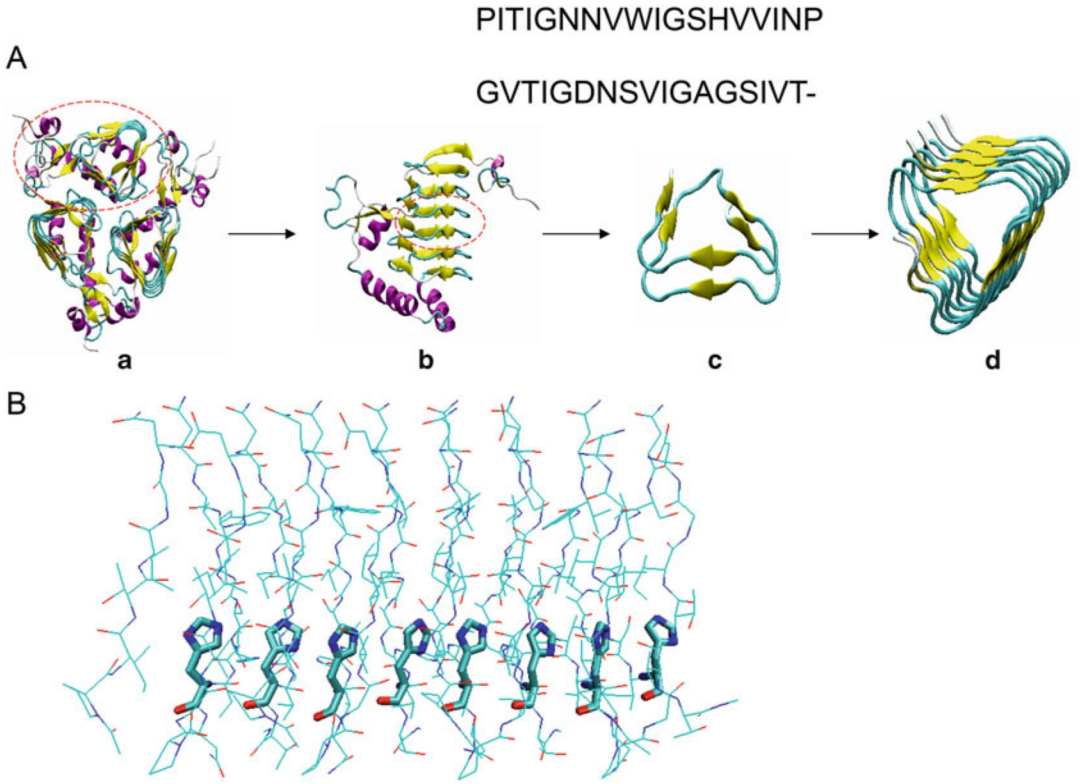

Fig. 2.

A schematic procedure of the construction of a nanotube using the naturally occurring protein building block from a β-helix (taken from galactoside acetyltransferase, PDB code: 1KRR). *Top*: (**a**) The trimeric crystal structure of galactoside acetyltransferase (GAT) from *E. coli*, with three left-handed parallel β-helix domains. (**b**) The monomeric structure of GAT (*circled*) taken from the trimeric GAT structure. (**c**) A single building motif (*circled*) taken from the monomeric 1KRR structure with selected residues 131–165. (**d**) A nanotubular structure obtained by stacking four repetitive building motifs on top of each other. *Bottom*: An example of one of the Histidine mutants

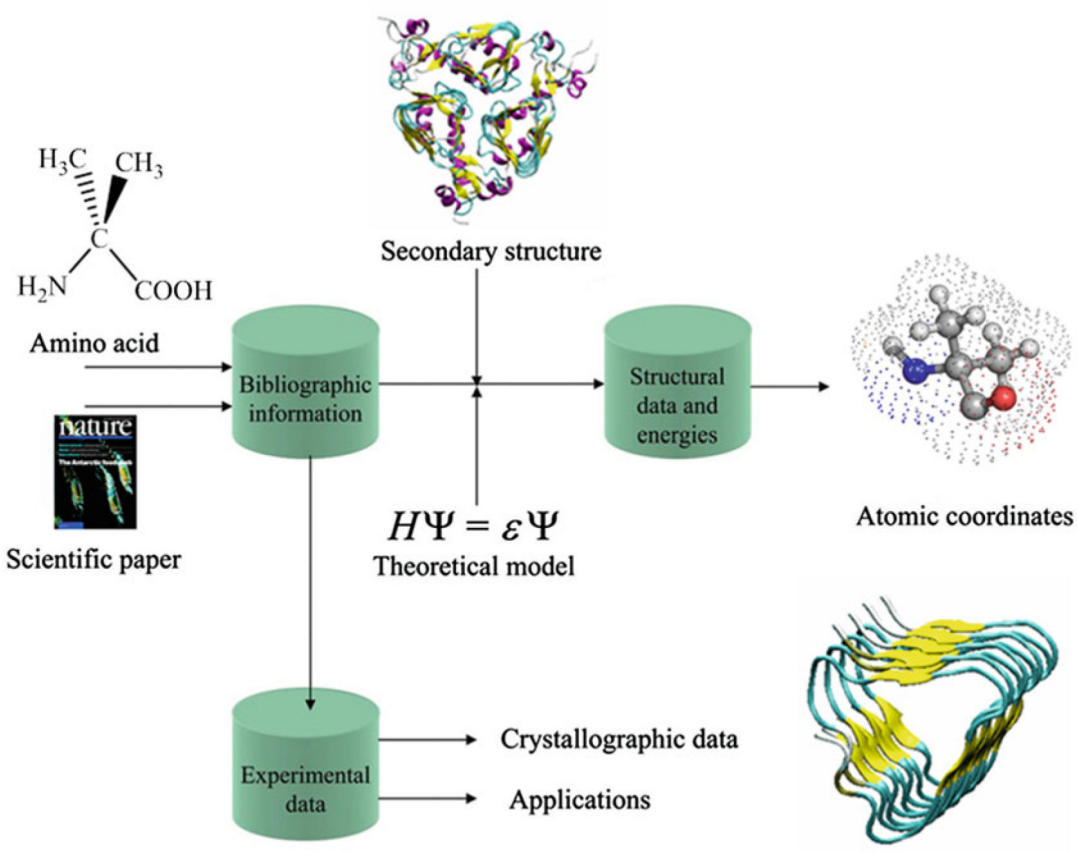

Fig. 3.
Schematic representation of the information flown in the NCAD database

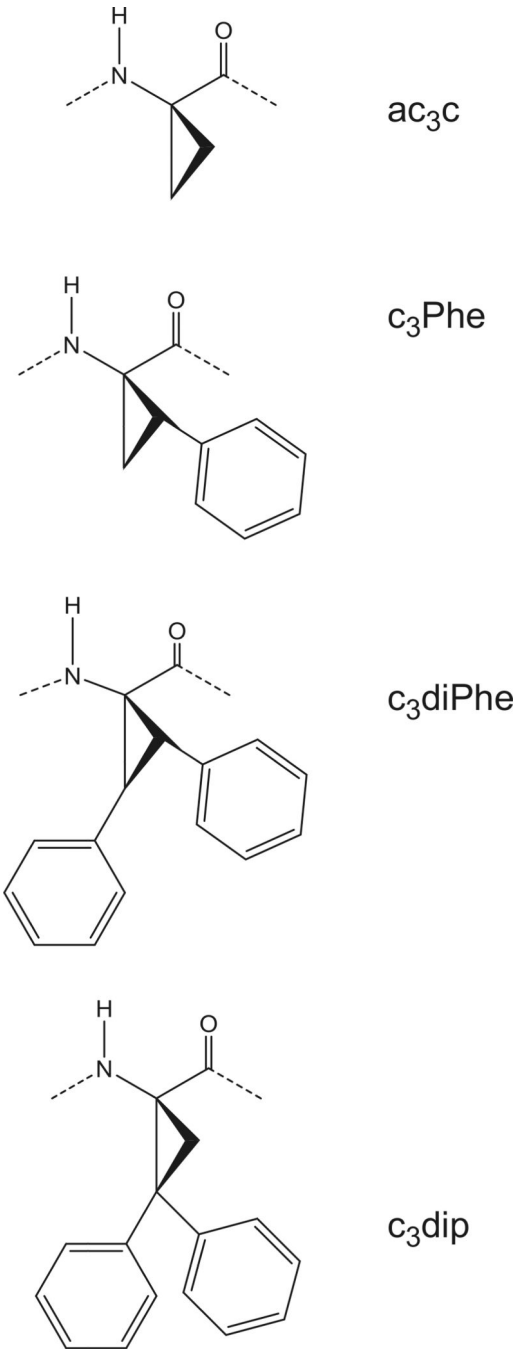

Fig. 4.
Illustration of the noncoding amino acids used in this study

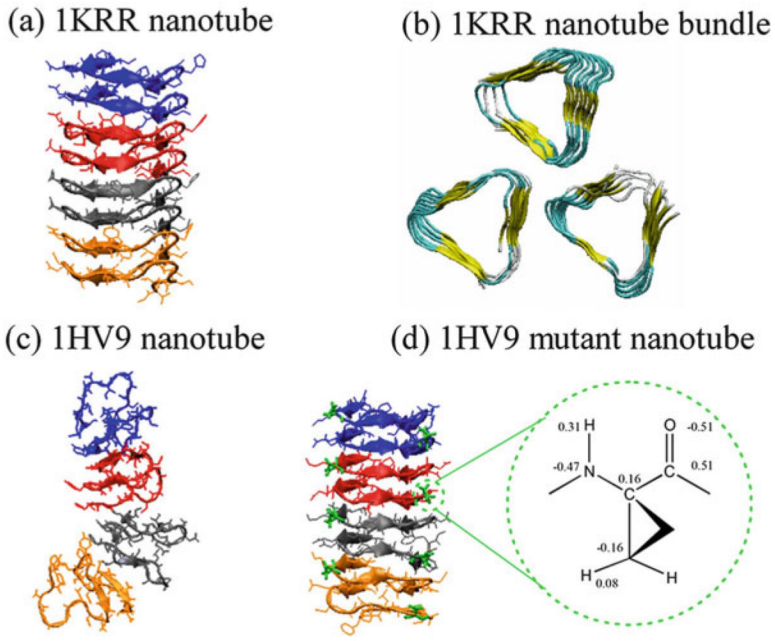

Fig. 5.

MD simulations of different nanotubes constructed by left-handed β-helical motifs. (**a**) 1krr nanotube and (**b**) 1krr nanotube bundle display high structural stability. (**c**) 1hv9 nanotube is not structurally stable. (**d**) Introduction of the conformationally restricted Ac3c residue in loop regions greatly enhances the stability of 1hv9 nanotube. Ac3c is displayed as a *green stick*

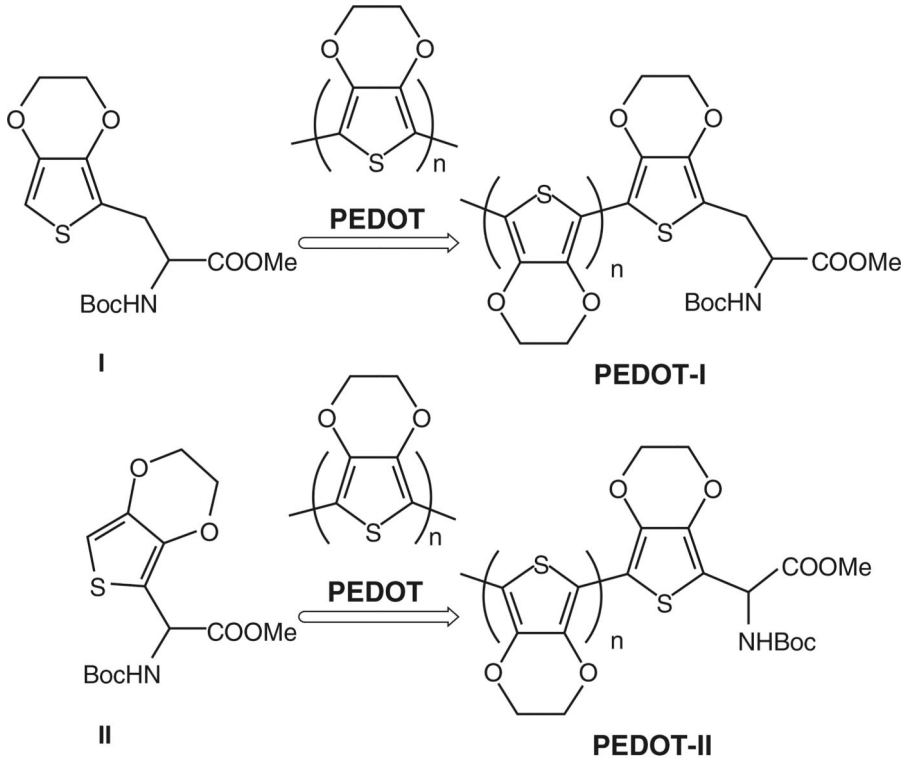

Scheme 1

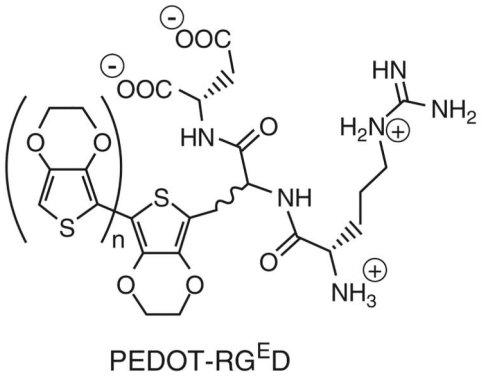

Scheme 2

Fig. 6.

(**a**) Synthesis of F–PLA and FF–PLA conjugates initiated by L-phenylalanine (H–Phe–OH) and L,L-diphenylalanine (H–Phe–Phe–OH). Taken with permission from ref. 87 (RSC Advances, 2014. 4(44): pp. 23,231–23,241); (**b**) Chemical structure of PEDOT-RG^{E}D

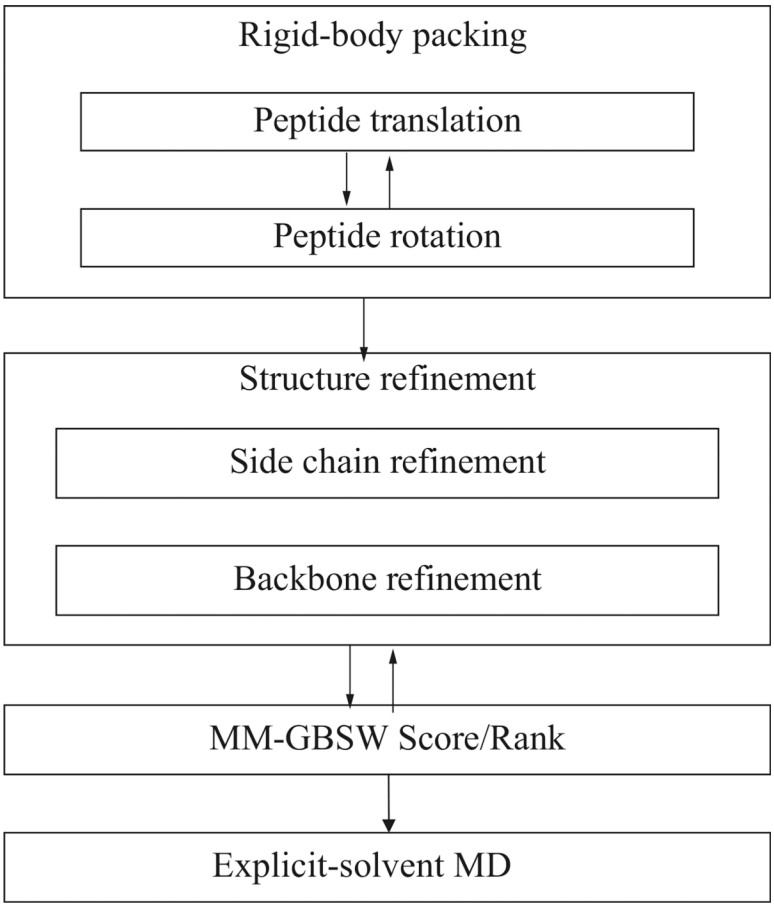

Fig. 7.
An overview of the peptide packing procedure

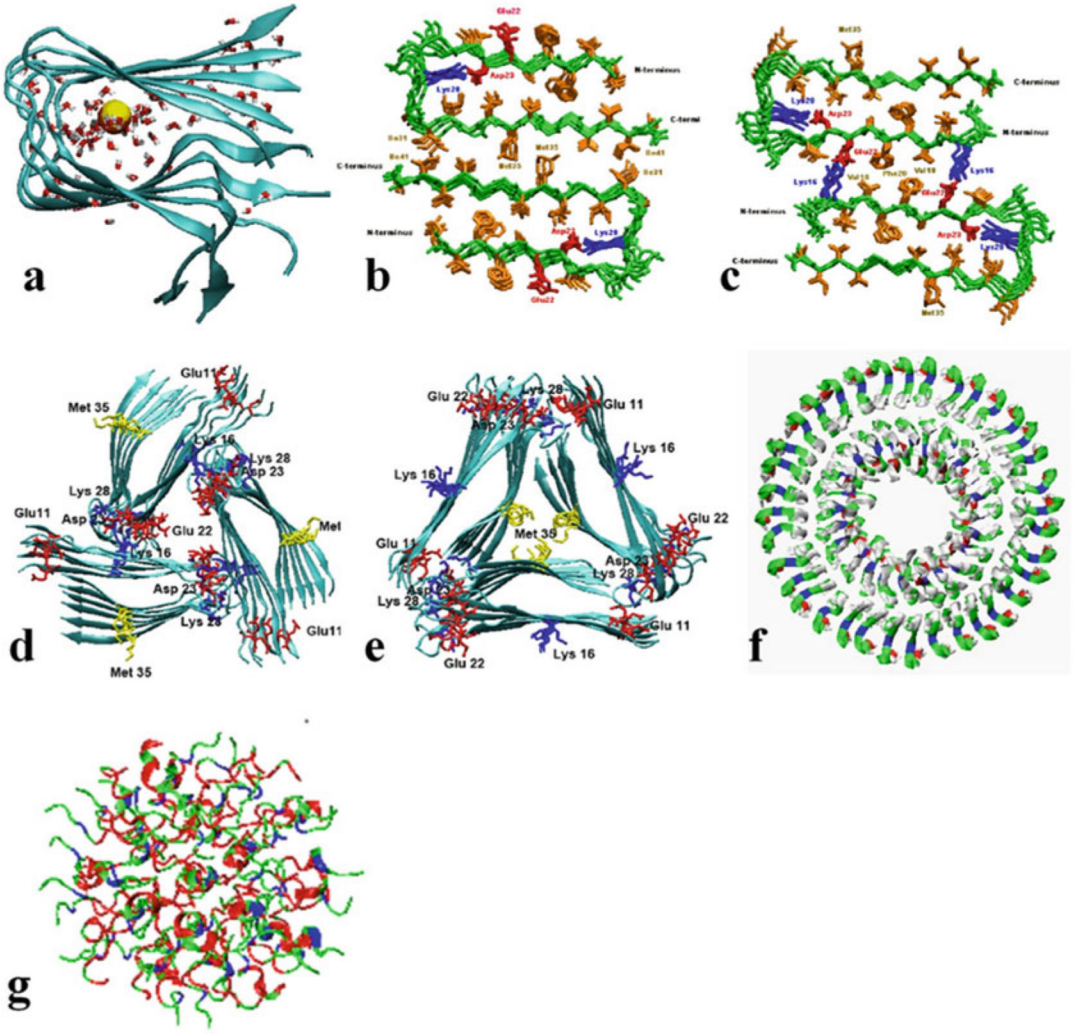

Fig. 8.

Atomic structures of amyloid oligomers formed by Aβ peptides. Each structure is computationally optimized and determined from thousands of conformers at the lowest energy state. Aβ oligomers include (**a**) single-layer linears; (**b, c**) double-layered linear, dimeric pentamers stacked in an antiparallel fashion via either C-terminal-C-terminal (CC) or N-terminal-N-terminal (NN) interface; (**d, e**) threefold triangular 18-mers with loop-next-to-tail or loop-next-to-strand organization; (**f**) double-layered annular 60-mer with the CC interface; (**g**) micelle with antiparallel peptide orientation

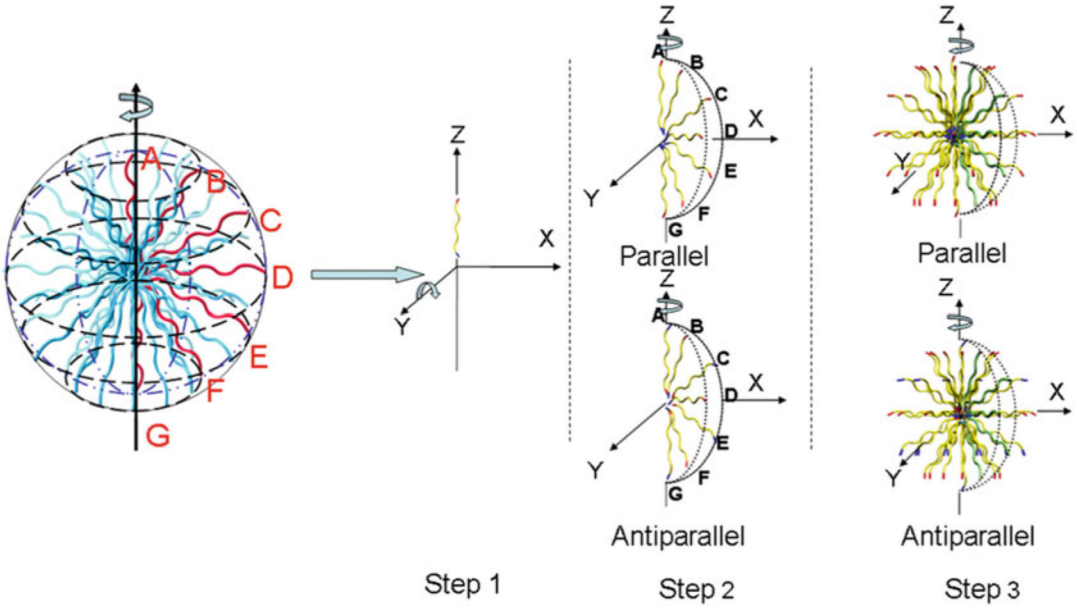

Fig. 9.

A three-step strategy to construct $A\beta_{25–35}$ micelles with parallel and antiparallel peptide orientations